CHEMISTRY OF MATERIALS

Article

pubs.acs.org/cm

Successive Layer-by-Layer Strategy for Multi-Shell Epitaxial Growth: Shell Thickness and Doping Position Dependence in Upconverting Optical Properties

Xiaomin Li, Dengke Shen, Jianping Yang, Chi Yao, Renchao Che, Fan Zhang,* and Dongyuan Zhao*

Department of Chemistry and Laboratory of Advanced Materials, Fudan University, Shanghai 200433, P.R. China

Supporting Information

ABSTRACT: One pot successive layer-by-layer (SLBL) strategy is introduced to fabricate the core/shell upconversion nanoparticles (NPs) for the first time by using high boiling-point Re-OA (rare-earth chlorides dissolved in oleic acid at 140 °C) and Na-TFA-OA (sodium trifluoroacetate dissolved in oleic acid at room temperature) as shell precursor solutions. This protocol is flexible to deposit uniform multishell on both hexagonal (β) and cubic (α) phase cores by successive introducing of the shell precursor solutions. Shell thickness of the obtained NPs with narrow size distribution (σ < 10%) can be well controlled from 1 monolayer (~0.36 nm) to more than 20 monolayers (~8 nm) by simply tuning the amounts of the shell precursors. Furthermore, the tunable doping positions (core doping and shell doping) can also be achieved by adjusting the species and addition sequence of the shell precursors. As a result of the high quality uniform shell and advanced core/shell structures, the optical properties of the obtained core/shell NPs could be improved in upconversion luminescence efficiency (up to 0.51 ± 0.08%), stability (more resistant to quenching by water) and multicolor luminescence emission.

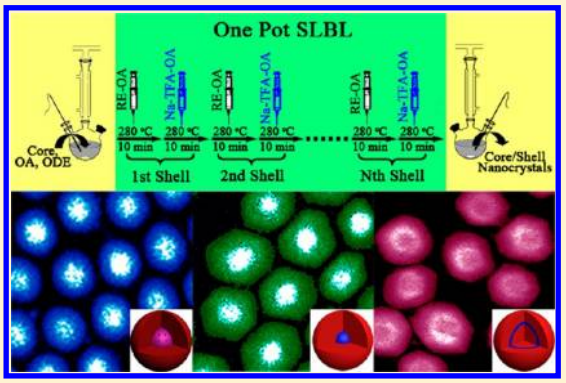

KEYWORDS: *core/shell, fluorescence, nanoparticles, upconversion*

Upconversion nanoparticles (UCNPs) have attracted a great deal of attention in bioapplications due to their high chemical stability, low toxicity, and high signal-to-noise ratio.[1−11] Despite the gains, many significant shortcomings certainly remain before their full potentials can be realized for practical applications, such as the low efficiency, surface quenching, and the lack of tunable emission.[12−14] To make up the deficiencies, growing a shell with small lattice mismatch around the core provides an effective way to improve the optical properties of the UCNPs.[14−18] However, recent work by van Veggel et al. shows that the core/shell nanoparticles (NPs) synthesized by the most widely used seed-mediated heat-up method do not have a uniform shell (the core is only partially covered by shell), which indicated that the core NPs cannot be passivated efficiently to decrease the core surface defects and insulated from the environmental effect.[19−21] On the other hand, it was found that the size distribution of the obtained core/shell NPs is larger than that of the original core. Furthermore, the bimodal size distribution was always observed when a high volume of shell precursors was introduced.[22] Although there have been a few reports on improving the photoluminescence stability of the rare-earth-based particles,[23] growing a uniform shell is still considered to be one of the most efficient routes to improve the stability of the UCNPs. Most recently, our group reported that a homogeneous shell could be obtained via a layer-by-layer epitaxial growth of shell by using the multicycle path, which was developed based on the widely used seed-mediated heat-up method (Scheme S1, Supporting Information).[24] The surface defects can be gradually passivated, which results in the obvious enhancement in overall UC emission intensity, lifetime, and more resistant to quenching by water molecules. However, owing to the selection of the low boiling point NaOH-NH_4F-methanol precursor, the multicycle path must undergo a lengthy cooling and volatile solvent removing process during the growth of every layer of shell. For the reason of batch operation, this process is considered to be time-consuming, laborious, and user unfriendly, especially for the synthesis of multishell (more than three) NPs.

Successive ion layer adsorption and reaction method has been demonstrated as an efficacious technique for growth of high quality core/shell II−VI semiconductor NPs.[25−29] The shell growth was designed to precisely control one monolayer (ML) by alternating injections of soluble precursors in high boiling-point solvent to the reaction mixture with core NPs at a high temperature. Based on this successive ion layer adsorption and reaction method, one pot successive layer-by-layer (SLBL) strategy is introduced to tune the structure/property of ternary compound UCNPs. In this context, the SLBL method is introduced to fabricate the core/shell UCNPs for the first time

Received: October 16, 2012
Revised: December 9, 2012
Published: December 10, 2012

Scheme 1. (A) SLBL Synthetic Procedure for the Core/Shell UCNPs. (B–D) Schematic Presentation for the Synthesis of Shell Thickness Controllable β-$NaGdF_4$:Yb,Er@$NaYF_4$ Core/Shell NPs (B), Core Doping α-$NaYbF_4$:Yb,Er@$NaYF_4$ (C), and Shell Doping α-$NaYF_4$@$NaYbF_4$: Yb,Er@$NaYF_4$ (D) Core/Shell/Shell NPs by using SLBL Method

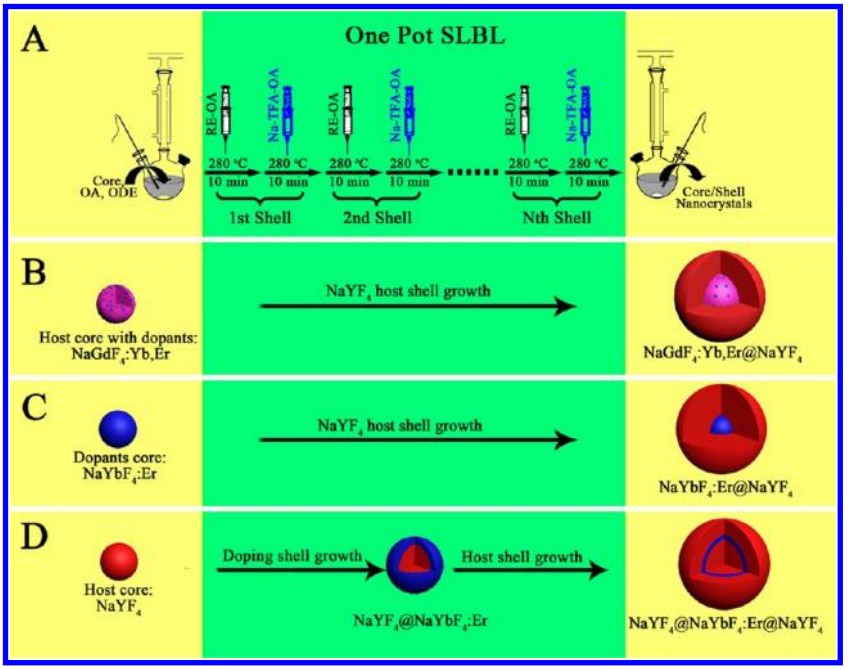

by using high boiling-point Re-OA (rare-earth chlorides dissolved in oleic acid at 140 °C) and Na-TFA-OA (sodium trifluoroacetate dissolved in oleic acid at room temperature) as shell precursor solutions (Scheme 1A). This protocol is flexible to deposit uniform (which means that the core NPs were entirely coated by the shells) multishell on both hexagonal (β) and cubic (α) phase core by successive introducing of the shell precursor solutions instead of the lengthy multicycle batch operation. Shell thickness of the obtained NPs with narrow size distribution (σ < 10%) can be well controlled from 1 ML (~0.36 nm)[24] to more than 20 ML (~8 nm) by simply tuning the amounts of the shell precursors. Furthermore, the tunable doping positions (core doping and shell doping) can also be achieved by adjusting the species and addition sequence of the shell precursors. As a result of the high quality uniform shell and advanced core/shell structures, the optical properties of the obtained core/shell NPs could be improved in UC luminescence efficiency (up to 0.51 ± 0.08%), stability (more resistant to quenching by water), and multicolor luminescence emission.

■ MATERIALS AND METHODS

Materials. Gadolinium(III) chloride anhydrous ($GdCl_3$, 99.99%), yttrium(III) chloride anhydrous (YCl_3, 99.9%), ytterbium(III) chloride anhydrous ($YbCl_3$, 99.9%), erbium(III) chloride anhydrous ($ErCl_3$, 99.9%), thulium(III) chloride anhydrous ($TmCl_3$, 99.9%), sodium trifluoroacetate (Na-TFA, 98%), 1-octadecene (ODE, 90%), oleic acid (OA, 90%), oleylamine (OAM, 70%), and polyvinylpyrrolidone 10000 g mol^{-1} (PVP 10000) were purchased from Sigma-Aldrich. Sodium hydroxide (NaOH, 96%), ammonium fluoride (NH_4F, 96%), and trifluoroacetic acid (TFA, 99%) were obtained from Beijing Chemical Reagents Co. Ltd. Yttrium(III) oxide (Y_2O_3, 99.99%), ytterbium(III) oxide (Y_2O_3, 99.99%), erbium(III) oxide (Er_2O_3, 99.99%), and thulium(III) oxide (Tm_2O_3, 99.99%) were obtained from Shanghai Yuelong Rare Earth New Materials Co., Ltd. All chemicals were used as received without any further purification.

Preparation of Shell Precursors. Y-OA host precursor: a mixture of YCl_3 (2.50 mmol), OA (10.0 mL), and ODE (15.0 mL) was loaded in a reaction container and heated at 140 °C under vacuum with magnetic stirring for 30 min to remove residual water and oxygen. Then, the colorless Y-OA precursor solution (0.10 M) was obtained. According to specific requirements, we could also prepare shell precursors with higher concentrations (such as 0.3 M). Yb-Er-OA and Yb-Tm-OA dopants precursor: The synthesis of Yb-Er-OA (0.10 M) and Yb-Tm-OA (0.10 M) were carried out all the same as that of Y-OA except 2.50 mmol of Yb-Er chloride (2.25 mmol of $YbCl_3$ and 0.25 mmol of $ErCl_3$) and 2.5 mmol of Yb-Tm chloride (2.475 mmol of $YbCl_3$ and 0.025 mmol of $TmCl_3$) were used instead of 2.5 mmol of YCl_3. Na-TFA-OA precursor: A mixture of Na-TFA (4.0 mmol) and OA (10 mL) was loaded in a container at room temperature under vacuum with magnetic stirring to remove residual water and oxygen. Then, the colorless Na-TFA-OA precursor solution (0.4 M) was obtained.

Synthesis of Core NPs. The synthesis of β phase $NaGdF_4$:Yb, Er core NPs, α phase core NPs with ($NaYbF_4$:Er) and without ($NaYF_4$) dopants in this work were similar to that previously reported (see the Supporting Information for the detailed synthesis process).[30,31]

Synthesis of β-$NaGdF_4$:Yb,Er@$NaYF_4$ Core/Shell NPs with Different Shell Thickness by using SLBL Method. In a typical process, 2.5 mL of the purified β-$NaGdF_4$:Yb,Er core cyclohexane solution (~4.5 nm, ~0.25 mmol) was mixed with 4.0 mL of OA and 6.0 mL of ODE. The flask was pumped down at 70 °C for 30 min to remove cyclohexane and any residual air. Subsequently, the system was switched to Ar flow, and the reaction mixture was further heated to 280 °C at a rate of ~20 °C/min. Then, 1 mL Y-OA (0.1 M) and 0.5 mL Na-TFA-OA (0.4 M) host shell precursors were alternately introduced by dropwise addition at 280 °C. Injection of shell precursor cycles could be performed to more than 20 cycles (Scheme 1A). The ripening time between each injection was kept at 15 min. The amounts and addition times of the shell precursor solutions could also be optimized according to specific requirements (the molar ratio of Y-OA to Na-TFA-OA precursors was 1:2). It means that the thickness of shell can be controlled not only with the multiple times layer-by-layer successive epitaxial shell growth by using low concentrations of the shell precursors but also with the single step shell growth by increasing the amount or concentration of the precursor solution (Figure 2). The

dx.doi.org/10.1021/cm3033498 | Chem. Mater. 2013, 25, 106–112

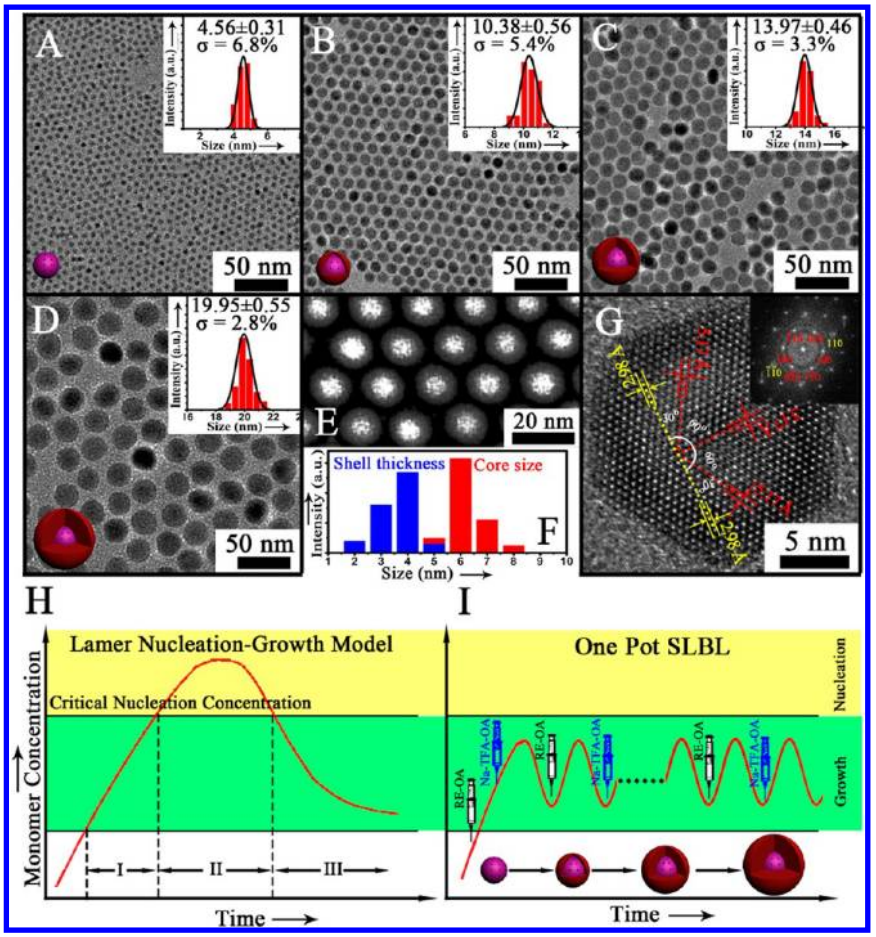

Figure 1. (A–D) TEM images and size distribution of β-$NaGdF_4$:Yb,Er core NPs and β-$NaGdF_4$:Yb,Er@$NaYF_4$ core/shell NPs with different shell thickness by using the SLBL method. The size distribution was represented by mean diameter ± standard deviation (more than 200 particles were compiled to obtain the mean diameter and standard deviation) (E–G) Typical HAADF-STEM, core size and shell thickness distributions, HRTEM image of the core/shell NPs. (H, I) Schematic illustration of Lamer plot and SLBL method for the controlled synthesis of core/shell UCNPs.

core/shell NPs were precipitated, washed, and dispersed in cyclohexane.

Synthesis of Core Doping α-$NaYbF_4$:Er/$NaYF_4$ core/shell UCNPs by using SLBL Method. Two milliliters of the purified α-$NaYbF_4$:Er core cyclohexane solution (~9 nm, ~0.2 mmol) were mixed with 4.0 mL of OA and 6.0 mL of ODE. The flask was pumped down at 100 °C with a mechanical pump for 30 min to remove any residual air and water. Subsequently, the system was switched to Ar flow, and the reaction mixture was further heated to 280 °C at a rate of ~20 °C/min for the injections. Then, 1 mL Y-OA (0.1 M) and 0.5 mL Na-TFA-OA (0.4 M) shell precursors were alternately introduced at 280 °C. The amounts and addition times of the precursors are listed in the Supporting Information, Table S1. The precursors were injected in a dropwise manner, and the time interval between each injection was 15 min. The core/shell NPs were precipitated, washed, and dispersed in cyclohexane.

Synthesis of Shell Doping α-$NaYF_4$@$NaYbF_4$:Er@$NaYF_4$ Core/Shell/Shell UCNPs by using SLBL Method. The preparative procedure for the cubic shell doping core/shell NPs was the same as the core doping NPs, except α-$NaYF_4$ NPs without dopants were used as the core instead of $NaYbF_4$:Er and the shell precursors were injected as needed for varied doping positions. In this process, a series of shell-doping core/shell NPs with different doping positions could be obtained by simply adjusting the addition sequence of dopants precursors and the host precursors. The amounts and injection sequences of the precursors for the synthesis of shell doping-I, shell doping-II, and shell doping-III were listed in the Supporting Information, Table S1. The core/shell NPs were precipitated, washed, and dispersed in cyclohexane.

Animal Experiments and in Vivo Imaging. Male Kunming mice (weighing 30–40 g) were purchased from Shanghai SLAC Laboratory Animal Co., Ltd. (Shanghai, China). All animal experimental procedures were in agreement with institutional animal use and care regulations. In vivo UCL imaging was performed with a modified LB983 NightOWL II (Berthold Technologies GmbH & Co.KG, Germany) using an external 0–2 W adjustable 980 nm CW laser as the excitation source. After the mice were anesthetized (with 100 μL of 10% chloral hydrate), the water-soluble UCNPs aqueous solution (100 μL, 1 mg/mL) in 0.9% NaCl saline solution was subcutaneously injected. Then, the optical whole body images of mice were recorded on the modified LB983 NightOWL II instrument.

Characterization. Transmission electron microscopy (TEM), high-resolution transmission electron microscopy (HRTEM), high-angle annular dark field imaging in the scanning TEM (HAADF-STEM), and electron energy loss spectroscopy (EELS) observations were performed on JEM-2100F transmission electron microscope with an accelerating voltage of 200 kV equipped with a postcolumn Gatan imaging filter (GIF-Tridium). X-ray diffraction (XRD) measurements were carried out at room temperature with a Bruker D8 diffractometer using Cu Kα radiation (wavelength = 1.5406 Å). The UC luminescence emission spectra were recorded on Hitachi Fluorescence Spectrometer F4500 instrument, but the excitation source used was an external 980 nm semiconductor laser (Changchun New Industries Optoelectronics Tech. Co., Ltd.) with an optic fiber accessory instead of the Xeon source in the spectrophotometer [All upconversion emission spectra were measured using the same laser power density (100 W/cm^{-2}) for excitation]. In vivo UCL imaging was performed with a modified LB983 NightOWL II (Berthold Technologies GmbH

dx.doi.org/10.1021/cm3033498 | Chem. Mater. 2013, 25, 106–112

& Co.KG, Germany) using an external 0−2 W adjustable 980 nm CW laser as the excited source.

RESULTS AND DISCUSSION

Three different core/shell structures with different crystal phases were designed to verify the feasibility of SLBL method: (a) shell thickness controllable synthesis of β phase $NaGdF_4$:Yb,Er@$NaYF_4$ core/shell NPs (Scheme 1B); (b) core doping of α phase $NaYbF_4$:Yb,Er@$NaYF_4$ core/shell NPs (Scheme 1C); and (c) shell doping of $NaYF_4$@$NaYbF_4$:Er@$NaYF_4$ core/shell/shell NPs (Scheme 1D). For the synthesis of shell thickness controllable β-$NaGdF_4$:Yb,Er@$NaYF_4$, a certain amount of β-$NaGdF_4$:Yb,Er cores were first synthesized based on a previous report.[30] Re-OA (rare-earth chlorides dissolved in oleic acid at 140 °C) and Na-TFA-OA (sodium trifluoroacetate dissolved in oleic acid at room temperature) host shell precursors were alternately introduced by dropwise addition at 280 °C afterward. Finally, β-$NaGdF_4$:Yb,Er@$NaYF_4$ core/shell NPs with different shell thickness were obtained by simply adjusting the amounts of the shell precursors. Core doping and shell doping processes were realized similarly except that the as-prepared α phase $NaYbF_4$:Er dopants cores and $NaYF_4$ host cores were used as the seed separately;[31] then, the corresponding shell precursors were alternately introduced to synthesis the doping position controllable core/shell NPs.

Transmission electron microscopy (TEM) images of β-$NaGdF_4$:Yb,Er core NPs and the corresponding β-$NaGdF_4$:Yb,Er@$NaYF_4$ core/shell NPs with different shell thicknesses (Figure 1A−D and Supporting Information Figure S1) show that the core NPs with a size of ∼4.5 nm has grown into larger NPs after the alternately introducing of the shell precursors. According to the size histograms obtained from the large area TEM images (Supporting Information, Figure S1), the size distributions of the obtained core/shell NPs are very narrow (σ < 10%), even after the particles are coated with nearly 20 ML of $NaYF_4$ shell. High-angle annular dark-field images combined with scanning TEM (HAADF-STEM), which is sensitive to atomic number (Z) contrast, is introduced to investigate the core/shell structure of the obtained NPs (Figure 1E and Supporting Information Figure S2). Owing to the much larger atomic number of Gd (Z = 64) compared with Y (Z = 39), a significant difference in contrast between the core (bright) and shell (dark) materials can be obviously observed, indicating successful growth of $NaYF_4$ shell onto the $NaGdF_4$:Yb,Er cores. It can be seen that the cores are completely covered by $NaYF_4$ shell, which is quite different from the nonuniform shell NPs synthesized by commonly used seed-mediated heat-up method (the core is only partially covered by shell).[14,19−21] The statistical results of the core size and shell thickness suggest the uniformity of the shell (Figure 1F). The d-spaces of the lattice planes measured from the high resolution TEM (HRTEM) image (Figure 1G) are ∼5.1 and ∼3.0 Å, with an angle of the two planes ∼30°, corresponding to the lattice parameters of the (100) and (110) planes of β phase $NaGdF_4$ or $NaYF_4$. The result is consistent with that of the selected area electron diffraction (SAED) and X-ray diffraction (XRD) patterns (Supporting Information, Figure S3).

To gain insights into the shell growth process, the plot of monomer concentration vs time in SLBL method is proposed (Figure 1I) based on the LaMer nucleation−growth model (Figure 1H). The Lamer plot is very useful for visualizing how the energy barrier works to induce the nucleation and growth.[32,33] As shown in Figure 1H, the concentration of "monomer", which is the minimum subunit of bulk crystal, constantly increases with time. The precipitation does not occur in stage I even under supersaturated conditions, because the energy barrier for spontaneous homogeneous nucleation is extremely high. In stage II, during which nucleation occurs, the degree of supersaturation is high enough to overcome the energy barrier for nucleation, thus resulting in the formation and accumulation of stable nuclei. Since the rate of monomer consumption resulting from the nucleation and growth processes exceeds the rate of monomer supply, the monomer concentration decreases until it reaches the critical nucleation concentration. Below this level, the system enters the growth stage (stage III), in which nucleation is effectively stopped and the particles keep growing as long as the solution is supersaturated. In SLBL method (Figure 1I), preformed nuclei are introduced into the reaction solution, then the shell precursors are alternately introduced, and the formed monomers are supplied to precipitate on the surface of the existing nuclei. The monomer concentration is kept low during growth to suppress homogeneous nucleation because its production and consumption maintains balance. So, the released monomers could be continuously consumed to deposit as shell without homogeneous nucleation. It should be noted that the seed particles need to be uniform to produce monodisperse core/shell NPs by using the SLBL method, which could also be concluded from the Supporting Information, Figure S4. Furthermore, it was found that the thickness of the shell can be controlled not only by the multiple times layer-by-layer successive epitaxial shell growth by using low concentrations of the shell precursors but also with the single step shell growth by increasing the amount or concentration of the precursor solution (Figure 2), which implies the high level of the critical nucleation concentration.

The fluorescence spectra of the core/shell NPs show a significant fluorescence enhancement during the growth of the $NaYF_4$ multishell, which results from the passivation of surface defects (Figure 3A). Remarkably, the quantum yield obtained

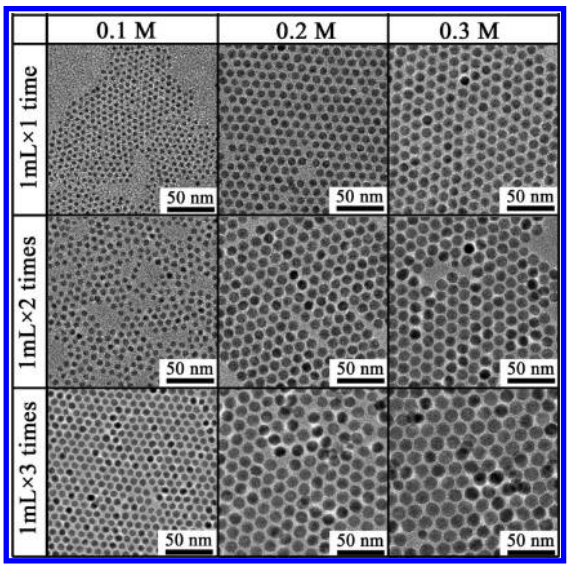

Figure 2. TEM images of the monodisperse β-$NaGdF_4$:Yb,Er@$NaYF_4$ core/shell NPs with different shell thicknesses that were synthesized by adjusting the number of addition times and the concentrations of shell precursors.

dx.doi.org/10.1021/cm3033498 | Chem. Mater. 2013, 25, 106−112

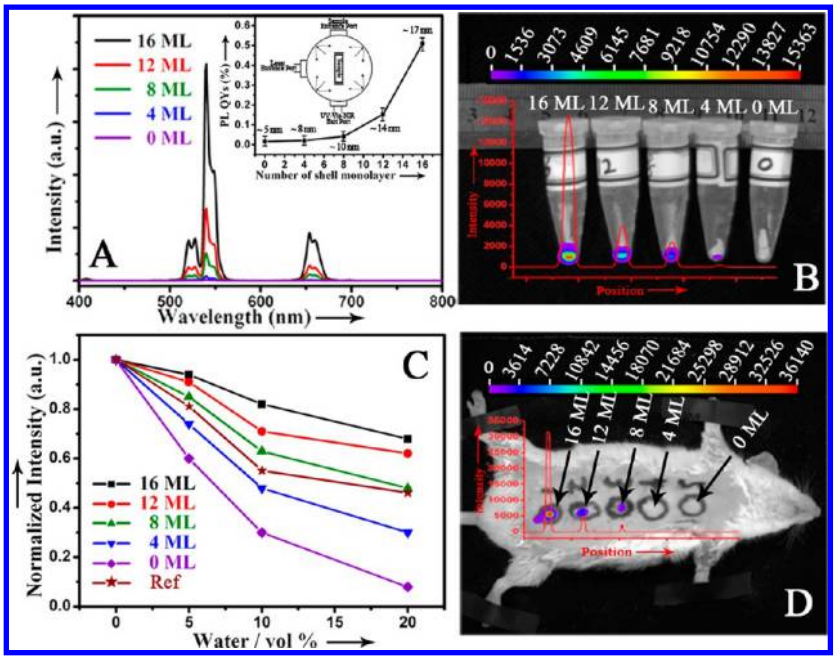

Figure 3. UC luminescence spectra (A) and fluoroscopic image (B) of β-$NaGdF_4$:Yb,Er@$NaYF_4$ core/shell NPs with different shell thickness. (C) Comparison of emission intensity loss in polar solvents with different amounts of water for core/shell NPs with different shell thickness obtained by SLBL method and conventional seed-mediated heat-up method. (D) In vivo UC luminescence imaging of mice after subcutaneous injections of water-soluble core/shell NPs with different shell thickness.

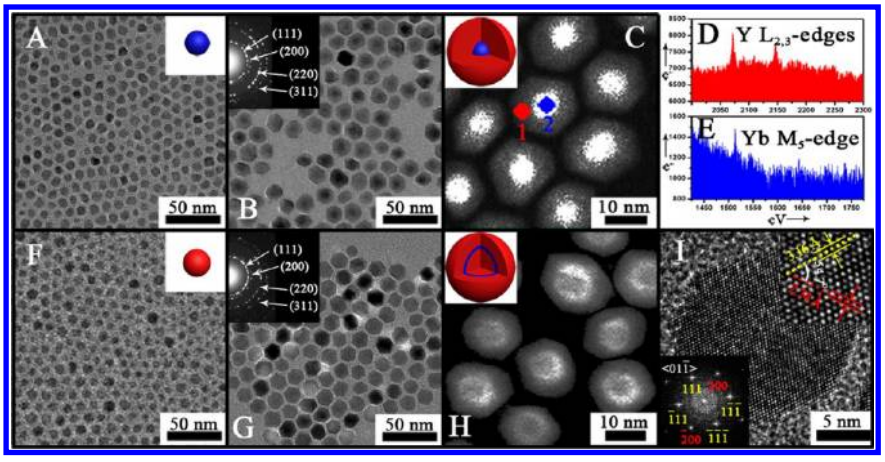

Figure 4. TEM images of the α-$NaYbF_4$:Er core (A), α-$NaYF_4$ core (F), core doping α-$NaYbF_4$:Er@$NaYF_4$ core/shell (B), and shell doping α-$NaYF_4$@$NaYbF_4$:Er@$NaYF_4$ core/shell/shell NPs (G) obtained by using the SLBL method. (C, H) HAADF-STEM images of the core doping and shell doping NPs. (D, E) EELS spectra of core doping NPs collected from the position 1 and 2 in (C). (I) Typical HRTEM image of the shell doping NPs.

by the integrated sphere is significantly increased from 0.016 ± 0.08% for the bare cores to 0.51 ± 0.08% when the shell thickness is increased to 16 ML (~6 nm). The fluoroscopic images of the core/shell NPs with different shell thickness further demonstrate that the fluorescence of the obtained core/shell NPs are significant improved as the shell thickness increases (Figure 3B). For the bioapplications, the UCNPs are always transferred to water solution by the ligand exchange method (Supporting Information, Figure S5).[34] It is found that more than 90% fluorescence of the bare core NPs undergoes dramatic quenching with the increase of water content to 20%, because of the high-energy stretching vibration effect of water molecule (Figure 3C). In stark contrast, the core/shell NPs obtained by SLBL method are found to be substantially more resistant to the quenching with an increase in shell thickness. When the shell thickness is over 8 ML (~3 nm), the obtained core/shell NPs is more resistant to quenching than the core/shell NPs obtained by conventional widely used seed-mediated heat-up method, which can attribute to the completely coverage of the uniform shell. It is important to note that nearly 30% fluorescence was quenched by water even after over coated with a 16 monolayer (~5.5 nm) shell (Figure 3C). We assume that the high-energy stretching vibration of the water molecule can be regarded as a surface oscillator. The interaction between this oscillator and the luminescence center (lanthanide ions) can also be realized without contacting. It means that the fluorescence can also be quenched by water with the noncontacting way, which is somewhat like the fluorescence resonance energy transfer (FRET).

dx.doi.org/10.1021/cm3033498 | *Chem. Mater.* 2013, 25, 106−112

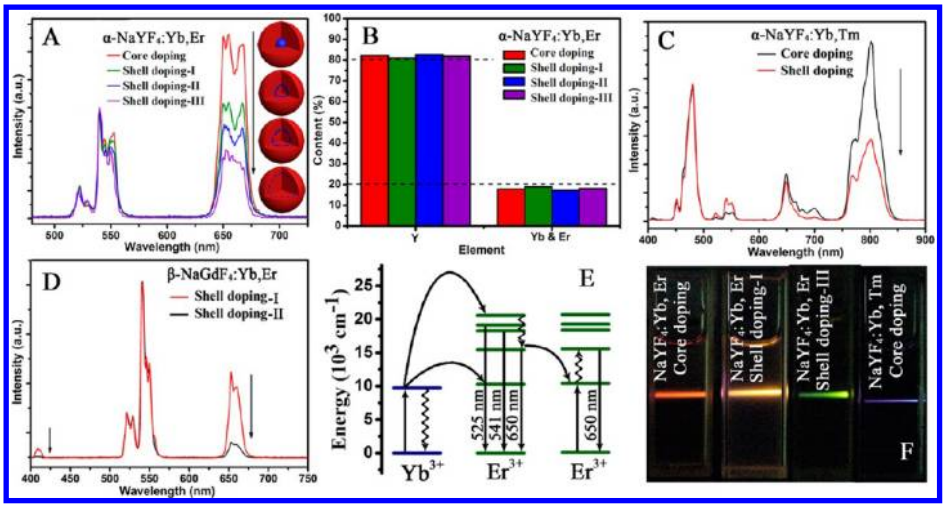

Figure 5. Fluorescence spectra of the Er based (A), Tm based (C) α phase core/shell NPs and β phase Er based core/shell NPs (D) with different doping positions. (B) Elemental compositions of lanthanide ions in the core doping α-$NaYbF_4$:Er@$NaYF_4$ core/shell, and shell doping α-$NaYF_4$@ $NaYbF_4$:Er@$NaYF_4$ core/shell/shell NPs determined by EDX. (E) Energy level schemes and energy transitions between Yb^{3+} and Er^{3+} and between Er^{3+} and Er^{3+}. (F) Optical photographs of the UCNPs with different doping positions (λ_{ex}= 980 nm, 5 W cm^{-2}).

Water-soluble $NaGdF_4$:Yb,Er@$NaYF_4$ core/shell NPs with different shell thicknesses are then employed as luminescent probes for in vivo imaging (Figure 3D). Dramatically increased UC luminescence signals are observed with the increase in shell thickness at the corresponding subcutaneous injection sites.

Based on the above discussion, we can confirm that the SLBL method is an effective way to fabricate high quality UCNPs with thickness controllable uniform shell. Since the simple and flexible advantages of SLBL method, we can further realize spatial position and local relative concentration (i.e., doping position) control of the dopants in a single nanocrystal (Scheme 1C and D), which may be another way to obtain multicolor emission UCNPs. So, core doping and shell doping UCNPs were first synthesized with delicate design and control. TEM images of the α-$NaYbF_4$:Er dopants core and the core doping α-$NaYbF_4$:Er@$NaYF_4$ core/shell NPs show a mean diameter of ~9 nm for the bare cores (Figure 4A and Supporting Information, Figure S7) and ~15 nm after coverage with $NaYF_4$ shell (Figure 4B). The *d*-spacings calculated from SAED patterns match well with interplanar distances of α phase $NaYbF_4$ or $NaYF_4$, which is consistent with the XRD results (Supporting Information, Figure S6). HAADF-STEM images show the significant difference in contrast, confirming the core/shell structure of the obtained core doping NPs (Figure 4C and Supporting Information, Figure S2). Electron energy loss spectroscopy (EELS) record from the probe location on the darker contrast region (marked with 1 in Figure 4C) shows Y $L_{2,3}$ edge signals (Figure 4D), while the Yb M_5 edge signal (Figure 4E) is detected on the brighter core region (marked with 2 in Figure 4C). These data clearly prove the core/shell structure of the core doping $NaYbF_4$:Er@$NaYF_4$ NPs. The size of the shell doping α-$NaYF_4$@ $NaYbF_4$:Er@$NaYF_4$ core/shell/shell NPs (Figure 4G) is also much larger than the bare α-$NaYF_4$ host core (Figure 4F), suggesting the epitaxial growth of the shell. In the synthesis process, a series of shell doping NPs with different doping positions can be obtained by simply adjusting the addition sequence of dopants and host precursors (Supporting Information, Figure S8). Further studies show that the size of the shell doping NPs are nearly the same as the core doping NPs (~15 nm) if the number of the shell precursors addition time is set to the same. HAADF-STEM results show a clear sandwich structure in contrast, confirming the core/shell/shell structure of the obtained shell doping NPs (Figure 4H). The α phase of the core and core/shell NPs is confirmed by HRTEM image (Figure 4I), XRD, and SAED patterns (Supporting Information, Figure S9). Combined with above results on the crystal structure of the obtained UCNPs, we can conclude that the crystal phase of the core/shell NPs obtained by SLBL method depends entirely on structure of the initial core. On the other hand, it is found that the size distribution of the obtained α phase core doping and shell doping NPs are broader than the β-$NaGdF_4$:Yb,Er@$NaYF_4$ core/shell NPs (Figures 1 and 2 and Supporting Information, Figures S1 and S11). As previously discussed, the size distribution of the obtained core/shell NPs is closely related to the size distribution of the core NPs, we attribute the cause of the broader size distribution to the nonuniform of the α phase core NPs (Supporting Information, Figure S7). However, the nonuniform of the core NPs could not affect the formation of the core/shell structure. So, we should not only focusing on the strategy for the fabrication of the core/shell UCNPs but also concentrating on the synthesis of high quality core NPs in the future work.

By comparing the fluorescence spectra of the core doping and shell doping NPs, the intensity ratio for red ($^4F_{9/2}$–$^4I_{15/2}$) to green ($^2H_{11/2}$–$^4I_{15/2}$, $^4S_{3/2}$–$^4I_{15/2}$) spectra (R/G) decreases prominently as the doping position gradually shifts from inner core to outer shell (Figure 5A). Similar phenomena can also be observed in other doping systems (Figure 5C and Supporting Information, Figure S10) and crystal structures (Figure 5D and Supporting Information, Figure S11). According to the literature report,[35] the decrease of R/G ratio in our synthesis is reasonable: when the same amount of dopants (Figure 5B) is doped in the different position of a consistent sized NPs, the local relative concentration of dopants can increase as the doping position is gradually transferred from outer shell to inner core. Due to efficient cross relaxation processes among the Er^{3+} ions at higher doping levels (Figure 5E), the R/G ratio can increase with the increasing local relative concentration of Er and Yb. Consequently, the doping position induced adjustable balance of emission intensities enables the NPs to display tunable fluorescent color output (Figure 5F), which

dx.doi.org/10.1021/cm3033498 | *Chem. Mater.* 2013, 25, 106–112

certifies the feasibility and effectiveness of the SLBL method from another aspect.

CONCLUSION

In summary, one pot successive layer-by-layer (SLBL) strategy is introduced to fabricate high-quality monodispersed core/shell UCNPs for the first time. This strategy is demonstrated to be a simple and effective way for the synthesis of both β phase and α phase uniform multishell upconversion NPs instead of the tedious multicycle batch operation. Shell thickness of the obtained NPs with narrow size distribution (σ < 10%) can be well controlled from 1 ML (~0.36 nm) to more than 20 ML (~8 nm) by simply tuning the amounts of shell precursors, which results in the significant improving on UC luminescence efficiency (up to 0.51 ± 0.08%) and stability (more resistant to quenching by water). Furthermore, tunable doping positions (core doping and shell doping) can also be achieved by adjusting the species and addition sequence of shell precursors to realize the multicolor emission. So, we believe that with the methodology of constructing high quality core/shell UCNPs reported in this paper, more and more advanced core/shell structure will be synthesized, which may turn over a new leaf in the nanolevel manipulation of UCNPs.

ASSOCIATED CONTENT

Supporting Information

Detailed process for the synthesis of β-$NaGdF_4$:Yb, Er, α-$NaYbF_4$:Er and α-$NaYF_4$ core NPs; Measurement of upconversion absolute quantum yield; Supporting figures and discussion on the obtained core/shell NPs by using the SLBL method. This material is available free of charge via the Internet at http://pubs.acs.org.

AUTHOR INFORMATION

Corresponding Author

*E-mail: dyzhao@fudan.edu.cn; zhang_fan@fudan.edu.cn.

Notes

The authors declare no competing financial interest.

ACKNOWLEDGMENTS

The work was supported by the NSFC (Grant Nos. 21101029, 21273041 and 21210004), China National Key Basic Research Program (973 Project) (No. 2013CB934100, 2012CB224805, 2010CB933901), Shanghai Rising-Star Program (12QA1400400), the State Key Laboratory of Pollution Control and Resource Reuse Foundation (No. PCRRF12001), and Fudan Startup Foundation for Advanced Talents. This work was also supported by Key Subjects Innovative Talents Program of Fudan University.

REFERENCES

(1) Zhang, F.; Braun, G. B.; Shi, Y. F.; Zhang, Y. C.; Sun, X. H.; Reich, N. O.; Zhao, D.; Stucky, G. *J. Am. Chem. Soc.* **2010**, *132*, 2850–2851.
(2) Jin, J.; Gu, Y. J.; Man, C. W. Y.; Cheng, J.; Xu, Z.; Zhang, Y.; Wang, H.; Lee, V. H. Y.; Cheng, S. H.; Wong, W. T. *ACS Nano* **2011**, *5*, 7838–7847.
(3) Zhang, F.; Braun, G. B.; Pallaoro, A.; Zhang, Y.; Shi, Y.; Cui, D.; Moskovits, M.; Zhao, D.; Stucky, G. *Nano Lett.* **2012**, *12*, 61–67.
(4) Zhang, F.; Haushalter, R. C.; Haushalter, R. W.; Shi, Y.; Zhang, Y.; Ding, K.; Zhao, D.; Stucky, G. *Small* **2011**, *7*, 1972–1976.
(5) Dai, Y.; Ma, P.; Cheng, Z.; Kang, X.; Zhang, X.; Hou, Z.; Li, C.; Yang, D.; Zhai, X.; Lin, J. *ACS Nano* **2012**, *6*, 3327–3338.
(6) Chen, Z. G.; Chen, H. L.; Hu, H.; Yu, M. X.; Li, F. Y.; Zhang, Q.; Zhou, Z. G.; Yi, T.; Huang, C. H. *J. Am. Chem. Soc.* **2008**, *130*, 3023–3029.
(7) Ostrowski, A. D.; Chan, E. M.; Gargas, D. J.; Katz, E. M.; Han, G.; Schuck, P. J.; Milliron, D. J.; Cohen, B. E. *ACS Nano* **2012**, *6*, 2686–2692.
(8) Bogdan, N.; Vetrone, F.; Ozin, G. A.; Capobianco, J. A. *Nano Lett.* **2011**, *11*, 835–840.
(9) Qian, H. S.; Guo, H. C.; Ho, P. C.; Mahendran, R.; Zhang, Y. *Small* **2009**, *5*, 2285–2290.
(10) Zhang, F.; Shi, Q.; Zhang, Y.; Shi, Y.; Ding, K.; Zhao, D.; Stucky, G. *Adv. Mater.* **2011**, *23*, 3775–3779.
(11) Xu, C. T.; Svenmarker, P.; Liu, H.; Wu, X.; Messing, M. E.; Wallenberg, L. R.; Engels, S. A. *ACS Nano* **2012**, *6*, 4788–4795.
(12) Boyer, J. C.; van Veggel, F. C. J. M. *Nanoscale* **2010**, *2*, 1417–1419.
(13) Wang, F.; Liu, X. *J. Am. Chem. Soc.* **2008**, *130*, 5642–5643.
(14) Wang, F.; Wang, J.; Liu, X. *Angew. Chem., Int. Ed.* **2010**, *49*, 7456–7460.
(15) Qian, H. S.; Zhang, Y. *Langmuir* **2008**, *24*, 12123–12125.
(16) Chen, F.; Bu, W.; Zhang, S.; Liu, X.; Liu, J.; Xing, H.; Xiao, Q.; Zhou, L.; Peng, W.; Wang, L.; Shi, J. *Adv. Funct. Mater.* **2011**, *21*, 4285–4294.
(17) Mai, H. X.; Zhang, Y. W.; Sun, L. D.; Yan, C. H. *J. Phys. Chem. C* **2007**, *111*, 13721–13729.
(18) Liu, Y.; Tu, D.; Zhu, H.; Li, R.; Luo, W.; Chen, X. *Adv. Mater.* **2010**, *22*, 3266–3271.
(19) Dong, C.; Korinek, A.; Blasiak, B.; Tomanek, B.; van Veggel, F. C. J. M. *Chem. Mater.* **2012**, *24*, 1297–1305.
(20) Abel, K. A.; Boyer, J. C.; Andrei, C. M.; van Veggel, F. C. J. M. *J. Phys. Chem. Lett.* **2011**, *2*, 185–189.
(21) Abel, K. A.; Boyer, J. C.; van Veggel, F. C. J. M. *J. Am. Chem. Soc.* **2009**, *131*, 14644–14645.
(22) Wang, F.; Deng, R.; Wang, J.; Wang, Q.; Han, Y.; Zhu, H.; Chen, X.; Liu, X. *Nat. Mater.* **2011**, *10*, 968–973.
(23) Cui, J.; Wang, Y.; Hao, J.; Caruso, F. *Chem. Mater.* **2009**, *21*, 4310–4315.
(24) Zhang, F.; Che, R.; Li, X.; Yao, C.; Yang, J.; Shen, D.; Hu, P.; Li, W.; Zhao, D. *Nano Lett.* **2012**, *12*, 2852–2858.
(25) Li, J. J.; Wang, Y. A.; Guo, W.; Keay, J. C.; Mishima, T. D.; Johnson, M. B.; Peng, X. *J. Am. Chem. Soc.* **2003**, *125*, 12567–12575.
(26) Xie, R.; Kolb, U.; Li, J.; Basché, T.; Mews, A. *J. Am. Chem. Soc.* **2005**, *127*, 7480–7488.
(27) Aharoni, A.; Mokari, T.; Popov, I.; Banin, U. *J. Am. Chem. Soc.* **2006**, *128*, 257–264.
(28) Embden, J.; Jasieniak, J.; Mulvaney, P. *J. Am. Chem. Soc.* **2009**, *131*, 14299–14309.
(29) Li, X.; Shen, H.; Li, S.; Niu, J. Z.; Wang, H.; Li, L. S. *J. Mater. Chem.* **2010**, *20*, 923–928.
(30) Johnson, N. J. J.; Oakden, W.; Stanisz, G. J.; Prosser, R. S.; van Veggel, F. C. J. M. *Chem. Mater.* **2011**, *23*, 3714–3722.
(31) Chen, G.; Ohulchanskyy, T. Y.; Kumar, R.; Ågren, H.; Prasad, P. N. *ACS Nano* **2010**, *4*, 3163–3168.
(32) LaMer, V. K.; Dinegar, R. H. *J. Am. Chem. Soc.* **1950**, *72*, 4847.
(33) Park, J.; Joo, J.; Kwon, S. G.; Jang, Y.; Hyeon, T. *Angew. Chem., Int. Ed.* **2007**, *46*, 4630.
(34) Johnson, N. J. J.; Sangeetha, N. M.; Boyer, J. C.; van Veggel, F. C. J. M. *Nanoscale* **2010**, *2*, 771–777.
(35) Kramer, K. W.; Biner, D.; Frei, G.; Gudel, H. U.; Hehlen, M. P.; Luthi, S. R. *Chem. Mater.* **2004**, *16*, 1244–1251.